Effect of Vortex Generators on NREL Wind Turbine
Aerodynamic Performance and Far-Field Noise

Ye, Qingqing; Avallone, Francesco; Van Der Velden, Wouter; Casalino, Damiano

Important note
To cite this publication, please use the final published version (if applicable).
Please check the document version above.

Effect of Vortex Generators on NREL Wind Turbine: Aerodynamic Performance and Far-Field Noise

To cite this article: Qingqing Ye *et al* 2020 *J. Phys.: Conf. Ser.* **1618** 052077

View the article online for updates and enhancements.

Effect of Vortex Generators on NREL Wind Turbine: Aerodynamic Performance and Far-Field Noise

Qingqing Ye[1], Francesco Avallone[2], Wouter van der Velden[3], Damiano Casalino[2]

[1]School of Aeronautics and Astronautics, Zhejiang University, 310058 Hangzhou, China

[2]Faculty of Aerospace Engineering, Delft University of Technology, 2629HS Delft, the Netherlands

[3]Dassault Systemes Deutschland GmbH, 70563 Stuttgart, Germany

qingqing_ye@zju.edu.cn

Abstract. Passive flow separation control with vortex generators (VG) is actively used over the wind turbine blade. In this paper, the effect of vortex generators is simulated on a full-scale 2-blade wind-turbine tested at the National Renewable Energy Laboratory. The simulation is performed using Very-Large-Eddy/Lattice-Boltzmann method (VLES/LBM). The analysis focuses on the effect of vortex generators on the aerodynamic performance and far-field noise. The simulation results without vortex generators are compared with the experimental results, reaching good agreement. The vortex generators produce counter-rotating vortices in the wake which effectively delay flow separation, leading to better aerodynamic performance. The acoustic analysis indicates that the dominant noise sources are the tonal noise produced by the flow separation and the turbulent-boundary-layer trailing-edge noise. Similar noise levels are obtained for the configurations with and without vortex generators.

1. Introduction

In the operation of wind turbine, the aerodynamic performance of the blade is highly degraded when flow separation occurs due to strong adverse pressure gradient. Flow separation and associated shear layer instability result in additional noise sources with impact on the far-field noise level. Vortex generators (VG) are widely used as passive flow control devices to delay or eliminate flow separation on the suction side of wind turbines [1]. Depending on the orientation of vortex generators, they typically produce co-rotating or counter-rotating vortices. The former vortices entrain high momentum fluid close to the wall; the resultant fuller boundary layer profile becomes less prone to flow separation. According to the experiment research performed by National Renewable Energy Laboratory (NREL) in 1996 [2], by mounting the vane shape VGs along the root area of the wind turbine, almost 5% increase of power output can be achieved at moderate freestream velocity. However, the cost of the VGs is drag penalty. The overall aerodynamic benefit strongly depends on the configuration of the VGs. Moreover, the VGs might also affect far-field noise. This aspect has not yet been assessed, especially for the full-scale wind turbine configuration due to the high cost.

In order to study the combined aeroacoustic and aerodynamic effects of VGs on a full-scale wind turbine, a 2-blade horizontal axis wind-turbine tested at the National Renewable Energy Laboratory (NREL) is

employed. The simulation is performed using Very-Large-Eddy/Lattice-Boltzmann method (VLES/LBM), which allows to perform simulation of large-scale model with complicate geometry at low computational cost. The validation of the simulation is performed by comparing pressure coefficient for the clean blade case with the experimental results. The far field noise of the wind turbine is estimated using Ffowcs-Williams and Hawking's (FW-H) analogy with unsteady pressure recorded at the permeable surfaces incorporating the contribution of blades, hub and tower as the input. Finally, the same NREL wind turbine is equipped with VG's to study the aerodynamic performance, as well as the impact on noise generation.

2. Computational method and noise estimation

The simulation is performed using the software package PowerFLOW 5.5b in which the discrete lattice Boltzmann equation is solved [3]. The velocity space is discretized into 19 velocities in three-dimensions (D3Q19 model), which corresponds to the direct numerical simulation of Navier-Stokes equations. In order to solve high-Reynolds number flow problems, a sub-grid scale model is implemented with a modified two-equation $k\text{-}\varepsilon$ renormalization group. The numerical domain is discretized into cubic volumetric elements. The equal spacing along three Cartesian axes between neighbouring elements increases the level of difficulty in fully resolving wall boundary layer. A hybrid wall model is implemented in the solver, which allows an accurate representation of near wall flow down to viscous sub-layer.

The noise prediction is performed with PowerFLOW, which is intrinsically unsteady and compressible. The acoustic pressure field can be extracted directly from the computational domain. In addition, in this work, the far-field noise is obtained by using a Ffowcs-Williams and Hawkings (FW-H) analogy [4, 5], where the sampling surface is fitted to a permeable surface surrounding the turbulent regime. The employed FW-H approach is based on a forward-time solution [6] of Farassat's formulation 1A [7], and available in 3DS's post-processing software PowerACOUSTICS.

3. Wind turbine model and simulation setup

The current simulation focuses on the flow and acoustic field around the horizontal axis two-bladed wind turbine. The model has been tested in NREL phase VI experiment campaign [8]. The turbine has an overall diameter of 10.058 m. The blade cross-section is a NREL S809 airfoil from root to tip with changing chord length and linear taper and nonlinear twist. The detailed description of the blade geometry can be retrieved from NREL phase VI report. The simulation is performed with the full-scale NREL wind turbine model. The wind turbine is operating at the 72 rpm, which is the same rotating speed as the experiment. The freestream velocity of $u_\infty = 10$ m/s is selected, representing the transient stall regime in the experiment. The vortex generator (VG) of vane shape is designed according to the optimization work on separation control [9], as shown in Figure 1. The arrangement and design of the vortex generator follows the recommendation proposed by Gyatt [9]. The VGs are mounted along 50% to 82% of the blade radius (R), and 10% of localized blade chord. The height (h) of the VG is 5 mm, which is 0.8 to 1.1% of the chord length over the blade. The incidence angle of the vane (β) is 15°. The width of the vane pair (d) is $4h$. The spacing between neighbouring span (D) is $8h$, leading to 39 VGs pairs over the entire blade radius.

The wind turbine geometry is centred in a simulation domain of 140R×100R×100R. The domain is larger than the real size of the wind tunnel to avoid blockage effect. A non-slip boundary condition is imposed at the wall. The spanwise and top ends of the domain have a slip wall condition, coving the side wall effect of the wind tunnel experiment. A pressure inlet and outlet conditions are imposed at the inlet and outlet of the domain. The pressure and temperature used are identical to the test conditions in the experiment. Acoustic sponge regions are placed at the outer part of the simulation domain. The former regions prevent the reflection of acoustic waves from the simulation boundaries, providing an anechoic condition. The grid generation process is fully automatic and follows a user defined Variable Resolution (VR) scheme. The finest mesh spacing around the VG is $\Delta x = \Delta y = \Delta z = 0.79$ mm, yielding 7 voxels over each VG height. For the blade, the finest mesh of the same size is placed around the

leading edge and trailing edge, corresponding to 12726 voxels across the rotor diameter (Figure 2). The resultant y^+ is 40. The blades and the hub are encompassed in a sliding mesh region.
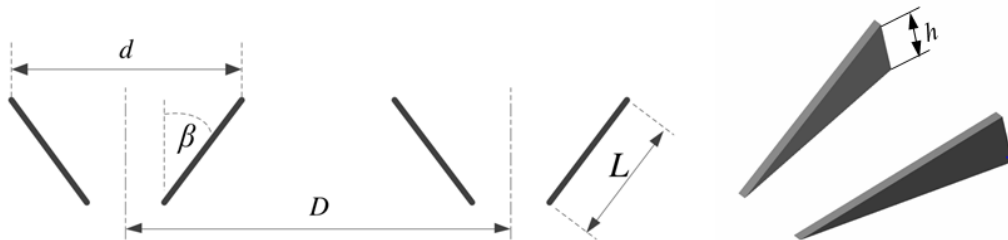

Figure 1. Geometry of vortex generator array, top (left) and perspective (right) view; height h = 5mm; vane angle β = 15°; vane length L = 4h; vane pair width d = 4h; vane pair spacing D = 8h.
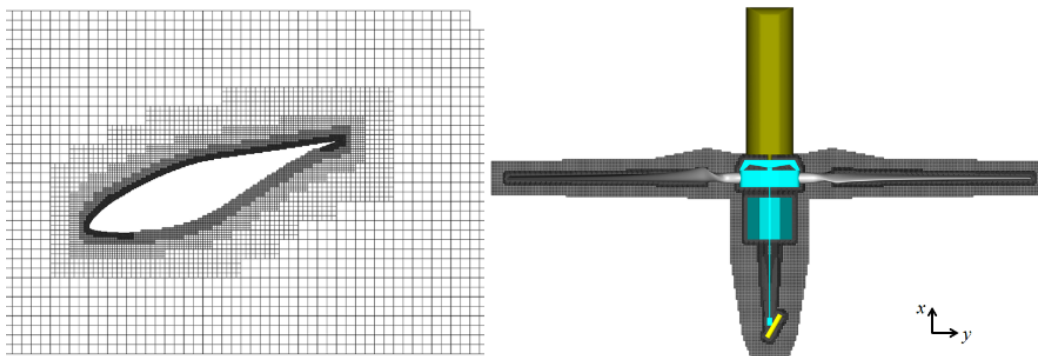

Figure 2. Simulation mesh around the blade cross-plane (left) and the sliding mesh region (right).

4. Wind turbine performance

The surface pressure coefficient distributions (c_p) for the configurations without and with VGs are presented in Figure 3 at three radial locations of r/R = 0.3, 0.63, and 0.8, respectively. For the baseline smooth blade, the simulated pressure coefficient shows good agreement with the experimental result at all radial locations, validating the accuracy of current result.

The VGs only influence the pressure distribution in the local radial range of the blade, as shown in Figure 3(b)(c). A grid convergence study is performed for the case with VGs. A fine resolution case is simulated with the minimum voxel size of 0.56 mm, yielding 10 cells per VG height. Good agreement has been found between the fine and mid grid case. As a result, the mid resolution case with $\Delta x = \Delta y = \Delta z$ = 0.79 mm finest voxel size is selected in the following analysis. Compared with the smooth configuration, the c_p rises from directly downstream of the VGs up to the chordwise location of x/c = 0.58 and 0.63 for r/R = 0.63 and 0.8, respectively. The former chordwise locations correspond to the local separation point, which will be further elaborated in the following section. Closer to the trailing edge, the pressure coefficient decreases slightly compared with the clean case.

The normal force coefficients (C_N) for both configurations are compared in Figure 4. For both cases, the C_N distributes non-uniformly along the radial direction, with higher value close to the root area. The VGs lead to the increase of normal force in the outboard region compared with clean blade case, indicating the local enhancement of aerodynamic performance.
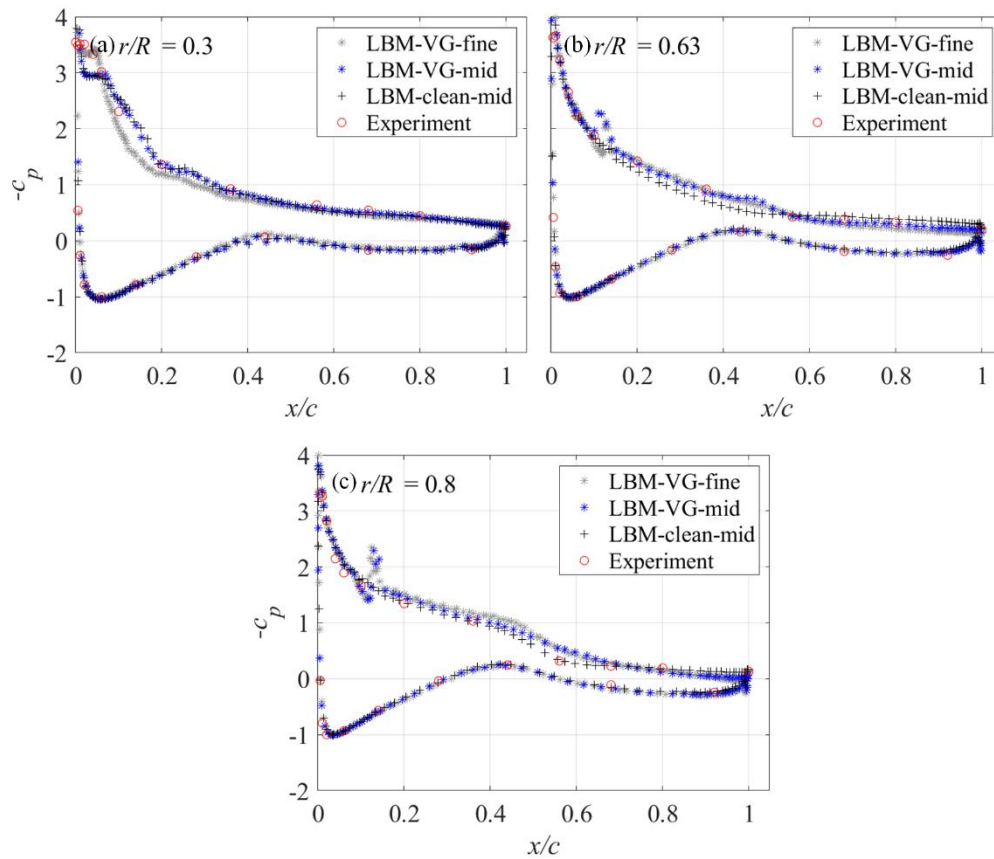
Figure 3. Pressure coefficient (c_p) at three radial locations, (a) $r/R = 0.3$, (b) $r/R = 0.63$, (c) $r/R = 0.8$.
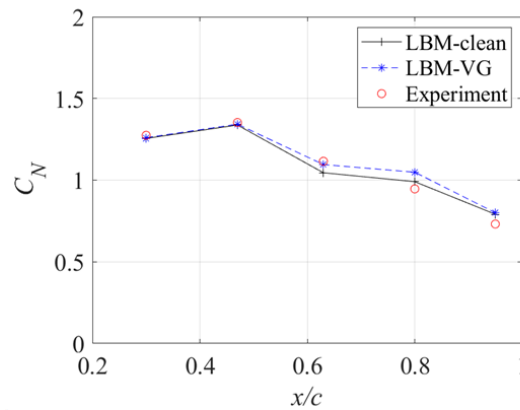

Figure 4. Normal force coefficient (C_N) distribution.

5. Flow field analysis

The first inspection of flow field around the full-scale wind turbine without/with VGs is shown in Figure 5 by the instantaneous vortical structures visualized by the iso-surface of λ_2, coloured by the axial velocity (u/u_∞). Similar flow structures are observed for both configurations. The coherent helical vortex structure sheds from the tip of the blades. The hub and nacelle induce strong disturbance to the flow, producing complex vortical structures in the surrounding area. Vortex shedding is produced from the trailing edge of the blade due to flow separation. The tower of the turbine leads to the shedding of Karman vortex sheet, which interacts with the helical vortex structure generated by the blade tip. For the case without VG, the Karman vortices undergo fast breakdown after the interaction. On the other

hand, the former vortical structures persist downstream for the case with VG mounted, convecting downstream with larger wavelength in the axial direction.
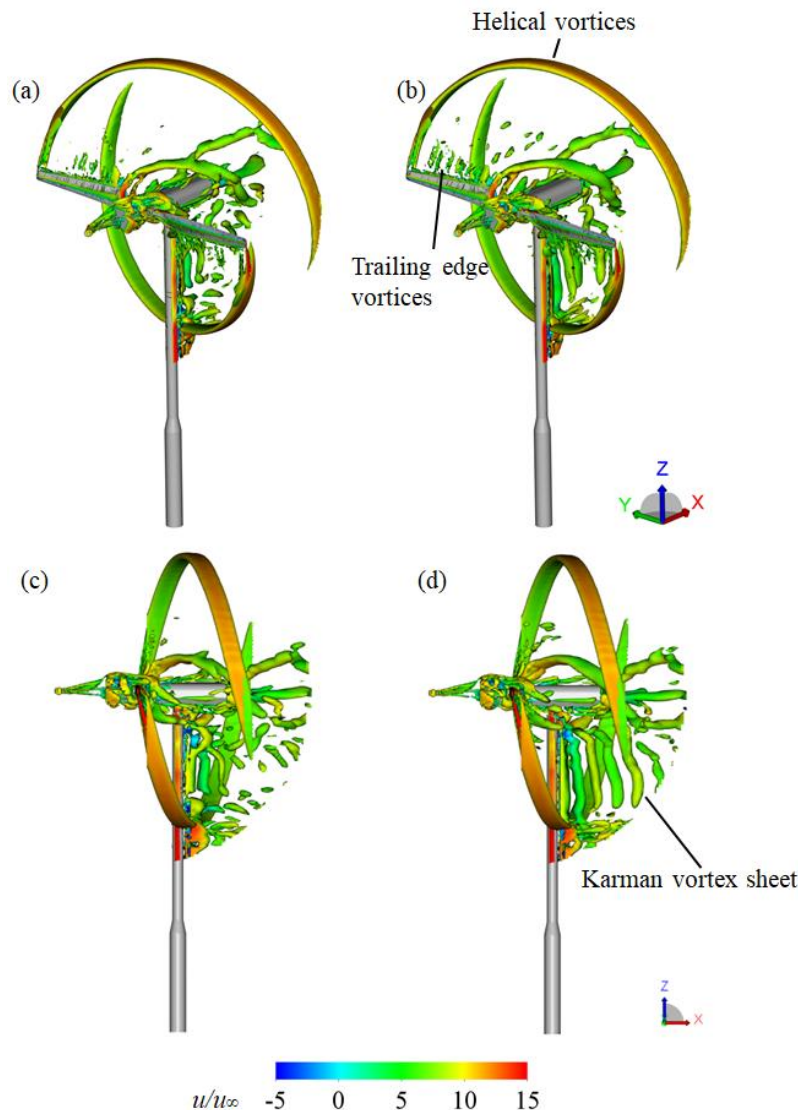

Figure 5. Instantaneous vortical field over the entire wind turbine visualized by the iso-surface of λ_2, coloured by the axial velocity, (a)(b): perspective view, (c)(d) side view, (a)(c): without VG, (b)(d): with VG.

To assess the effect of the VGs on the flow, instantaneous flow field over the suction side of the blade is shown in Figure 6 by surface streamlines. For the baseline smooth blade configuration (see Figure 6(a)), the flow along the inner part of the blade separates from the leading edge and shows strong radial velocity component. Moving towards blade tip, the separation line gradually moves downstream towards the trailing edge. From $r/R = 0.85$ on, the flow becomes fully attached. When the VG array is mounted on the blade (Figure 6(b)), flow separation is delayed of approximately 10% of the local chord length when the radial location $r/R > 0.53$. On the contrary, flow separation moves slightly upstream towards the leading edge closer to the blade root ($r/R = [0.50\ 0.53]$).

Further inspection into the vortical structures over the suction side of the blade indicates strong vortex shedding from the trailing edge of the blade due to flow separation for the baseline configuration, as

shown by the iso-surface of of λ_2 criterion (Figure 7). The periodicity and strength of the vortices significantly depend on the strength of the flow separation. The recirculation zone shows strong correlation in the radial direction. When the VG array is mounted on the blade (Figure 7(b)), counter-rotating vortices are produced downstream of VGs, transporting high momentum fluid flow to the blade surface, which delays the separation. The spanwise shear layer of the separation area interacts with counter-rotating vortices, leading to localized large-scale vortical structures close to the separation line. The circulation zone in the radial direction is distorted due to the vortical interaction, yielding weaker radial correlation. If the less correlated flow structures persist to the trailing edge, the noise level could be mitigated compared to the clean baseline configuration [10]. The VGs show better effect on separation delay towards the blade tip, revealing the dependence of relative distance between the VGs and the separation line at local radial location [11, 12]. The relative distance affects the strength of the VG produced vortices at the separation line and the momentum transportation effect.
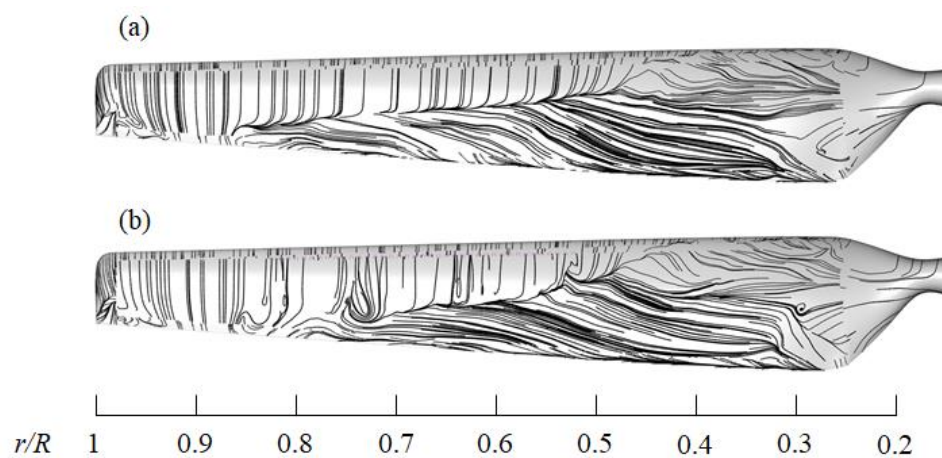

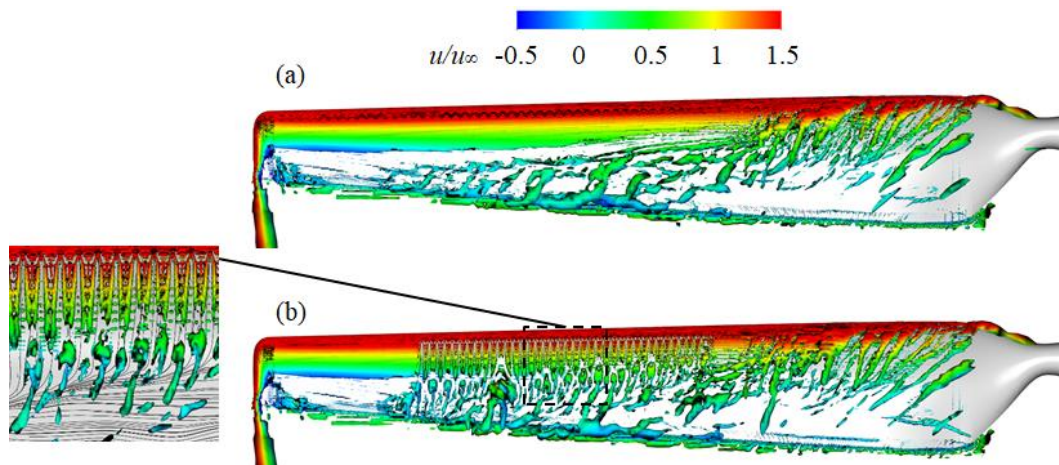Figure 6. Surface streamline distribution over the suction side of blade without (a) and with (b) VG.

Figure 7. Instantaneous vortical field over the suction side of the blade visualized by the iso-surface of λ_2, coloured by the axial velocity, (a) without VG, (b) with VG.

6. Far-field noise analysis

The far-field noise is computed using the Ffwocs-Williams and Hawkings acoustic analogy using the data computed on a circular array of microphones in $x - z$ plane at $2R$ from the centre of the wind turbine with a spacing of 10°, yielding 36 microphones over the circle. In the analysis, the contributions of the blades, nacelle, hub and tower are included. The Overall Sound Pressure Level (OSPL) in the plane is calculated, as shown in Figure 8, in which 0° corresponds to the downstream axial direction. The OSPL

is integrated in the frequency domain of [10, 5000] Hz. Compared with smooth blade configuration, the VGs show negligible effect on far-field noise level. In the range of 0° to 120°, similar noise levels are obtained. The directivity indicates a maximum noise level at 70°, which is 20 dB larger than the minimum level in the upstream axial direction of 180°.

To provide further insight to the acoustic field, the sound pressure level (L_p) at three microphone locations, namely 0°, 90° and 180°, is calculated against frequency with a bandwidth of 10 Hz, as shown in Figure 9. Similar sound pressure spectra are produced for the configurations without and with VG. For these two cases, high noise level is produced in the low frequency band ($f < 1500$ Hz), following a decaying broadband energy in the higher frequency range. The broadband noise is related to the turbulent-boundary-layer trailing-edge noise [13]. Slightly higher narrow band noise level is found in the range of 350 Hz to 600 Hz for the VG case. Multiple tones are amplified, associating with noise generated by flow separation and shear layer instability. Two fundamental tones locate at the peak frequencies of $f_1 = 465$ Hz and $f_2 = 1500$ Hz and their first harmonic are shown in all three microphone locations. The peak at f_1 and its first harmonic have lower sound pressure level for the microphones at 90° and 180°, in agreement with the observation from the directivity of OSPL (see Figure 8). The former observation on the noise generation mechanism is supported by the time-derivative of surface pressure over the suction side, as shown in Figure 10. The results reveal that the noise sources mainly locate at the flow separation area and trailing edge.
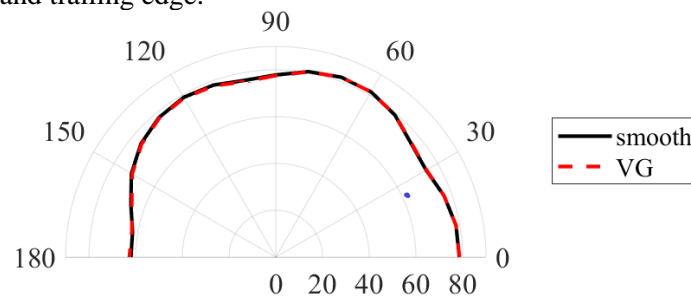

Figure 8. Overall Sound Pressure Level (OSPL) obtained from a circular array of microphones at 2*R*.
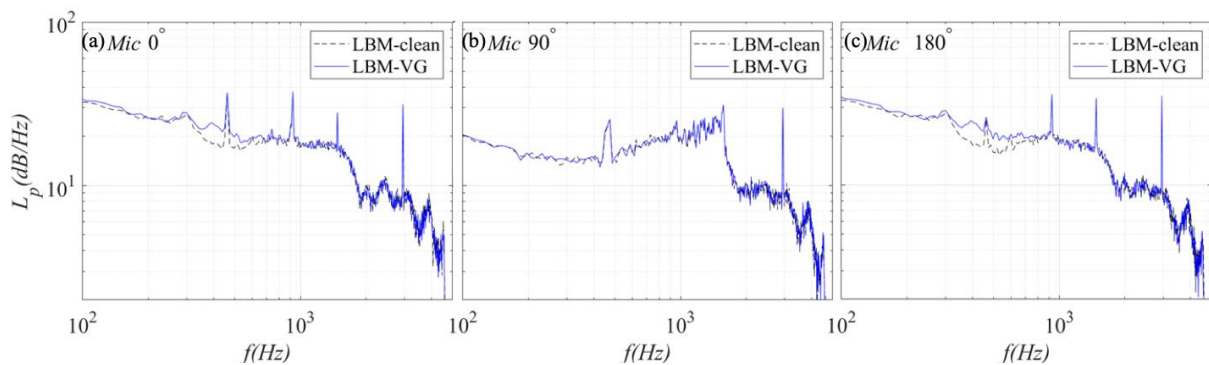

Figure 9. Sound pressure level (L_p) obtained from three microphones located at 2R from the centre of the wind turbine, (a) 0°, (b) 90° (c) 180°.
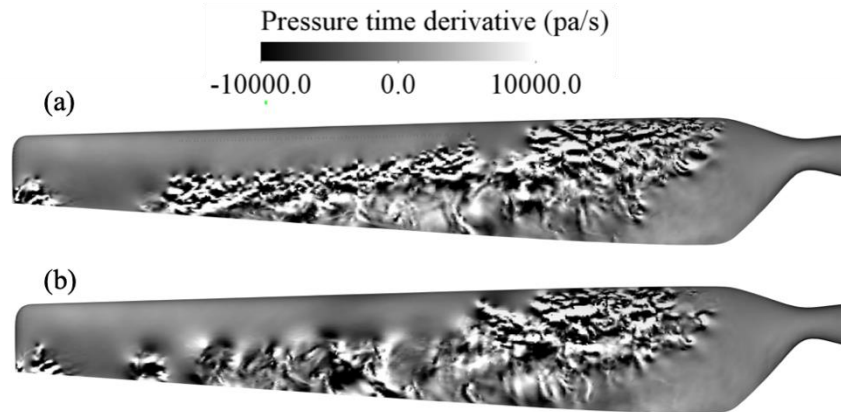
Figure 10. Time derivative of the surface pressure over the suction side, (a) without VG, (b) with VG.

The noise source for the tones is confirmed by the RMS of bandpass filtered surface pressure fluctuations. The RMS of non-filtered surface pressure fluctuations are shown in Figure 11 (a-1)(b-1) for reference. The RMS of pressure fluctuation component is filtered at the centre frequency of $f_1 = 465$ Hz and $f_2 = 1500$ Hz, as shown in Figure 11(a-2)(b-2) and (a-3)(b-3) respectively. For the non-filtered cases (see Figure 11 (a-1)(b-1)), high level of surface pressure fluctuations is observed at where the flow is separated over the suction side of the blade. The maximum fluctuation level is produced close to the separation line. Due to the interaction between the counter-rotating vortices produced by the VGs with the shear layer of the separation bubble, the line-shaped peak transforms into localized spots (see Figure 11 (b-1)). Another pressure fluctuation peak is produced at the blade tip, relating to the helical vortex. When the surface pressure fluctuations is filtered at $f_1 = 465$ Hz, high level of surface pressure fluctuations focuses in the area around the separation line, indicating that the tonal noise is produced by the flow separation and shear layer instability. The VGs lead to higher fluctuation levels over the downstream separation line. The tip vortices also contributes to the noise generaton at the former frequeuncy. For the frequency of $f_2 = 1500$ Hz, the same origins of pressure fluctuation peaks are observed compared with f_1, showing lower peak magnitude.
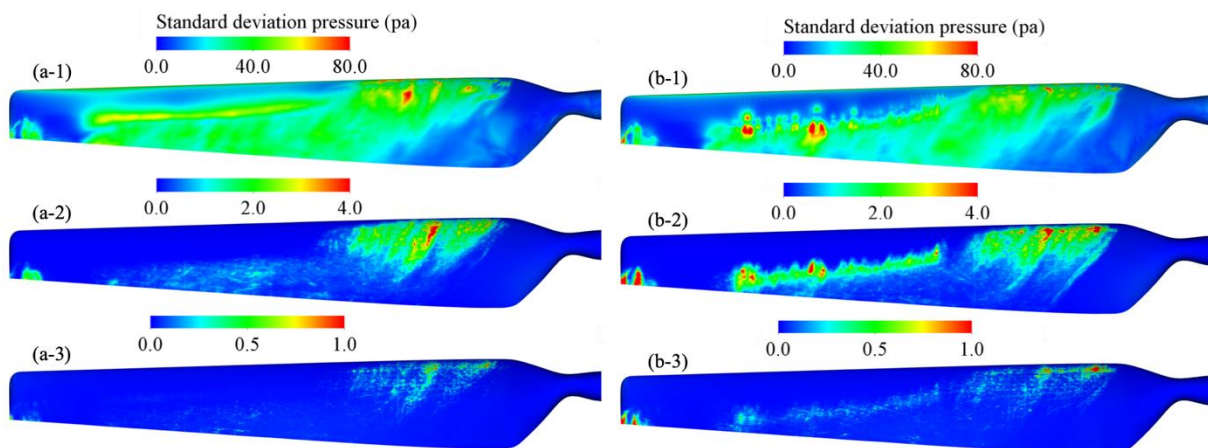

Figure 11. RMS of surface pressure fluctuations, (a) without VG, (b) with VG, 1: non-filtered, 2: band-pass filtered at $f_1 = 465$ Hz, 3: band-pass filtered at $f_1 = 1500$ Hz.

7. Conclusion
In the current study, the effect of vortex generators (VGs) on aerodynamic and aeroacoustic performance of the full-scale 5 MW NREL is investigated using Very-Large-Eddy/Lattice-Boltzmann method (VLES/LBM). Two configurations without and with VGs mounted are simulated at the freestream velocity of 10 m/s, corresponding to the transient stall regime if the NREL wind turbine. Good

agreement has been obtained between the simulation and experimental results for the configuration without VGs, validating the feasibility of the simulation.

The instantaneous flow organization around the VGs immersed in three-dimensional incoming boundary layer shows the formation of counter-rotating vortices in the wake, transporting high momentum fluid toward the blade surface. Flow separation is effectively delayed in the outboard part of the blade, improving the aerodynamic characteristics.

Two main sources are detected to contribute to far-field noise of the wind turbine both without and with VGs. One is the flow separation and shear layer instability over the suction side of the blade, leading to multiple tonal noises at low and moderate frequencies. The other is the turbulent-boundary-layer trailing-edge noise, causing broadband sound pressure level amplification in the low frequency range ($f < 1000$ Hz). The presence of VGs has trivial effect on overall sound pressure level and directivity. The simulation results indicate that the VGs have the potential to improve the aerodynamic performance without causing noise penalty.

References

[1] Lin J C 2002 *Progress in Aerospace Sciences* **38** 389.
[2] Griffin D A 1996 *Investigation of vortex generators for augmentation of wind turbine power performance*. National Renewable Energy Lab., Golden, CO (United States); Lynette (R.) and Associates, Seattle, WA (United States).
[3] Casalino D, Ribeiro A F P, Fares E and Nölting S 2014 *AIAA J.* **52** 1232.
[4] Brès G, Pérot F and Freed D 2010 *16th AIAA/CEAS Aeroacoustics Conference*.
[5] Najafi-Yazdi A, Brès G A and Mongeau L 2010 *Proceedings of the Royal Society A: Mathematical, Physical and Engineering Science*
[6] Casalino D 2003 *Journal of Sound and Vibration* **261** 583.
[7] Farassat F and Succi G P 1982 *The prediction of helicopter rotor discrete frequency noise*, *In: American Helicopter Society, Annual Forum, 38th, Anaheim, CA, May 4-7, 1982, Proceedings.(A82-40505 20-01) Washington, DC, American Helicopter Society, 1982, p. 497-507.*, pp. 497.
[8] Hand M, Simms D, Fingersh L, Jager D, Cotrell J, Schreck S and Larwood S 2001 *Unsteady aerodynamics experiment phase VI: wind tunnel test configurations and available data campaigns*. National Renewable Energy Lab., Golden, CO.(US).
[9] Gyatt G 1986 *Development and testing of vortex generators for small horizontal axis wind turbines*. AeroVironment, Inc., Monrovia, CA (USA).
[10] Ye Q, Avallone F, Ragni D, Choudhari M M and Casalino D 2019 *Effect of Surface Roughness on Boundary Layer Transition and Far Field Noise*, *25th AIAA/CEAS Aeroacoustics Conference*.
[11] Giepman R H M, Schrijer F F J and van Oudheusden B W 2014 *Physics of Fluids* **26** 066101.
[12] Baldacchino D, Ferreira C, Tavernier D D, Timmer W A and Bussel G J W 2018 *Wind Energy* 1.
[13] Brooks T F, Pope D S and Marcolini M A 1989 *Airfoil Self-Noise and Prediction*. NASA technical report.